Characterization of the molecular iodine electronic wave functions and potential energy curves through hyperfine interactions in the $B0_u^+(^3\Pi_u)$ state

Lisheng Chen, Wibe A. de Jong,* and Jun Ye

JILA, National Institute of Standards and Technology and Department of Physics, University of Colorado, Boulder, Colorado 80309-0440

Received October 18, 2004; revised manuscript received December 5, 2004; accepted December 13, 2004

We present a high-resolution analysis of the six electronic states that share the same dissociation limit with the second excited electronic state B in molecular iodine. These six states are coupled to the B state via hyperfine interactions. The four hyperfine parameters, C_B, δ_B, d_B, and eqQ_B, are calculated with the available potential energy curves and wave functions constructed from the separated-atom basis set. We obtain a maximum separation of the respective contributions from all six electronic states and compare each individual contribution with high-precision spectroscopic data, providing an independent verification of the relevant electronic structure. © 2005 Optical Society of America

OCIS codes: 020.2930, 300.6390, 300.6460, 300.6190.

1. INTRODUCTION

Comprehensive and high-precision measurements on hyperfine spectra in the $B \leftarrow X$ system of molecular iodine provide a unique opportunity for a detailed examination of the molecule's electronic structure relevant to the second dissociation limit, $^2P_{3/2}+^2P_{1/2}$. Molecular iodine is a rare case in that the hyperfine spectra in the $B \leftarrow X$ system have been recorded not only with high precision at the kilohertz level but also for a large set of rovibrational levels, extending from $v'=2$ to just below the dissociation limit ($v'=82$) in the excited $B0_u^+(^3\Pi_u)$ electronic state.[1–17] Precise empirical–interpolation formulas have been developed to describe the hyperfine interaction.[2,3] These interpolation forms present a detailed frequency map for precision measurements relying on the hyperfine spectrum of molecular iodine. The vibrational levels studied cover a broad range of internuclear separation, with R centroid (R_c, the mean of internuclear separations weighted by the B-state vibrational wave function) ranging from approximately 3 to 12 Å. Because hyperfine interactions can exert large influences on electronic structure, experimentally determined hyperfine parameters over a large range of R_c allow a sensitive test of the relevant electronic wave functions and potential energy curves.

Precise measurement of hyperfine interactions has been applied to test several relevant electronic states, i.e., X, B, and E in molecular iodine[4,18–25] and in other diatomic molecules.[26] In the case of the $B0_u^+(^3\Pi_u)$ state in molecular iodine, second-order contributions to the four hyperfine parameters, the electric quadrupole parameter eqQ_B, spin–rotation parameter C_B, tensorial spin–spin parameter d_B, and scalar spin–spin parameter δ_B, have been calculated for several vibrational levels ($v' \sim 40-82$) in the B state.[4,18,19,22–24] In these analyses, the molecular wave functions involved were constructed from a separated-atom basis set because the molecule spends much of its time at large internuclear separations for high-lying vibrational levels close to the dissociation limit. The good agreement between the experimental data and these calculations justifies the separated-atom model as a simple and effective tool in characterizing the electronic structure at large internuclear separations. Nonetheless, there is room to extend this approach. First, the same calculation can be carried out with improved resolution for vibrational levels lower than $v' \sim 40$ as well as for the detailed rotational dependence in each vibrational level. This approach has become particularly relevant given the latest spectroscopic data with an extensive coverage of vibrational and rotational dependence of the hyperfine interactions.[16,17] In addition, detailed information on the short- and intermediate-range ($R<7$ Å) potential energy curve (PEC) of the perturbing electronic state, obtained either empirically or theoretically, was largely unavailable when these earlier calculations were performed, and therefore the property of the molecular wave function of the corresponding electronic state could not be independently inferred from these analyses. In contrast, with adequate constraints on the PECs, a correct account of the hyperfine parameters permits either the determination of the admixture of the basis wave functions in the separated-atom model or the verification of more sophisticated molecular wave functions.

In this paper, we extend the calculation of hyperfine parameters to low vibrational levels and to rotational dependence at each vibrational level, using electronic wave functions derived from the separated-atom basis set and the related empirical or theoretical PECs. Our aim is to

0740-3224/05/050951-11/$15.00

take advantage of our recently measured hyperfine parameters covering an extensive range of rovibrational levels near the dissociation limit[16,17] and combine them with other published experimental data to test the PECs, the electronic wave functions, and the separated-atom model. In doing so, we are able to quantitatively address several issues such as (1) to what extent the separated-atom wave functions can be extrapolated to small internuclear separations, (2) the estimation of the admixture of the basis wave functions in the separated-atom model, and (3) the sensitivity of the dependence of hyperfine parameters on the choice of PECs. For the spin–rotation parameter C_B, the calculated dependence on both vibrational and rotational quantum numbers is in good agreement with the experimental data for $v' \geqslant 42$. Subsequently, the admixture of the two 1_u states is independently determined. Moreover, calculations of the other three parameters, eqQ_B, d_B, and δ_B, place a stringent constraint on the long-range PECs of the relevant electronic states. Here we consider the smooth second-order contributions. Thus the calculation does not cover the abnormal variations of the hyperfine parameters around $v'=57-60$ and $v'=76-78$, for which the existence of the strong hyperfine coupling has already been analyzed in a great detail.[4,16,23]

In Section 2 we introduce the explicit form of the second-order contributions to the hyperfine parameters in Hund's case c coupling scheme, along with a discussion of the PECs and the electronic wave functions in the separated-atom model. We present results for the four effective hyperfine parameters at various internuclear separations in Section 3. These results are discussed in three steps to demonstrate the maximum separation of contributions from different perturbing electronic states. First, a detailed analysis of C_B is required for the determination of the admixture of the two 1_u states. Then, through the calculation of δ_B, contributions from the other two states (0_u^- and 0_g^-) are separated from the rest (two 1_g states), and the corresponding long-range PECs are tested. Finally, we present results for eqQ_B and d_B, which are in part based on the information derived in the previous two steps. Conclusions are provided in Section 4.

2. THEORY

The hyperfine interaction, which is not included in the Born–Oppenheimer molecular Hamiltonian, can couple the $B0_u^+$ state to several electronic states sharing the same $^2P_{3/2}+^2P_{1/2}$ dissociation limit.[27,28] Consequently, the hyperfine spectra of the $X \leftarrow B$ transitions are altered to various degrees depending on the coupling strength and the energy differences between the $B0_u^+$ and the perturbing states. An effective Hamiltonian based on second-order perturbation theory was developed by Broyer *et al.*[28] to treat these couplings. Except for levels at which strong coupling is present, perturbed hyperfine spectra can generally be described by the effective hyperfine Hamiltonian with high precision by use of the four effective hyperfine parameters, eqQ_B, C_B, d_B, and δ_B, extracted from fitting the spectroscopic data to the effective Hamiltonian. Moreover, second-order calculations of these parameters relate their experimental values to the relevant PECs and the admixture of the basis wave functions, imposing stringent constraints on the relevant electronic structure.

The detailed derivation of the matrix elements of this effective hyperfine Hamiltonian and the associated effective hyperfine parameters can be found in the literature.[24,28] For clarity of the notation and discussion, we provide an overview of this derivation before we list the explicit expressions. Then we proceed to describe several computational issues concerning the preparation of the PECs, the electronic wave functions constructed from the separated-atom basis set, and the electronic matrix elements.

A. Matrix Element of the Hyperfine Hamiltonian

The hyperfine Hamiltonian of the iodine molecule can be formally written as

$$H_{\mathrm{hf}} = H_{\mathrm{hf}}(a) + H_{\mathrm{hf}}(b) + H_{\mathrm{hf}}(a,b), \tag{1}$$

where a and b denote the two iodine nuclei and $H_{\mathrm{hf}}(a)$ [$H_{\mathrm{hf}}(b)$] and $H_{\mathrm{hf}}(a,b)$ represent the nucleus–electron and nucleus–nucleus hyperfine interactions, respectively. The last term in the above Hamiltonian is left out in the following discussion because it contains only nuclear coordinates and thus cannot couple different electronic states. With the last term dropped, this Hamiltonian can be expressed in tensorial form:

$$H_{\mathrm{hf}} = \sum_{\alpha=a,b} \sum_{k} \sum_{q=-k}^{k} (-1)^q Q_q^k(\mathbf{I}_\alpha) V_{-q}^k(e_\alpha), \tag{2}$$

where the rank-k spherical tensor operators $Q^k(I_\alpha)$ and $V^k(e_\alpha)$ act, respectively, on the nuclear spin $\mathbf{I}_\alpha$ and the electronic degrees of freedom.

Considering the strong spin-orbit interaction in this heavy molecule, Hund's case c coupling scheme at large internuclear separations is appropriate for the molecular basis set, which we denote by

$$|\psi\rangle = |\Omega v J I F M_F\rangle, \tag{3}$$

where Ω is the projection of the total angular momentum $\mathbf{J}$ onto the molecular axis connecting the two nuclei, v is the vibrational quantum number, $\mathbf{I}$ is the total nuclear spin, $\mathbf{F}=\mathbf{I}+\mathbf{J}$, and M_F is the projection of $\mathbf{F}$ onto a quantization axis. Note that in the energy continuum, the discrete level index v is replaced by a continuous energy spectrum E. Averaging explicitly over the molecular rotation in the laboratory frame gives matrix elements of this hyperfine Hamiltonian in terms of $3j$ (parentheses) and $6j$ (curly brackets) symbols and electronic matrix elements:

$$\begin{aligned}\langle \psi' | H_{\mathrm{hf}}^k(a) | \psi \rangle = {} & \delta_{FF'} \delta_{M_F M_F'} (-1)^{F+\Delta I+2I_a+\Delta J+k} [(2J'+1) \\ & \times (2J+1)(2I'+1)(2I+1)]^{1/2} \begin{pmatrix} J' & k & J \\ -\Omega' & \Delta\Omega & \Omega \end{pmatrix} \\ & \times \begin{Bmatrix} J' & k & J \\ I & F & I' \end{Bmatrix} \begin{Bmatrix} k & I_a & I_a \\ I_a & I' & I \end{Bmatrix} f_k(a, \Omega', v_{J'}', \Omega, v_J),\end{aligned} \tag{4}$$

where $\Delta J = J' - J$, $\Delta I = I' - I$, $\Delta\Omega = \Omega' - \Omega$, and $f_k(a, \Omega', v_{J'}', \Omega, v_J)$ encapsulates the averaging over the

electronic motion in the molecular frame and the molecular vibration, which is written as

$$f_k(a,\Omega',v'_{J'},\Omega,v_J)=(-1)^{\Omega'}\frac{C_k}{\begin{pmatrix} k & I_a & I_a \\ 0 & I_a & -I_a \end{pmatrix}}\langle \Omega' v'_J|V^k_{\Delta\Omega}(a)|\Omega v_J\rangle. \tag{5}$$

Here $C_1=\mu_N g_{I_a} I_a$ is the nuclear magnetic dipole moment, where μ_N is the nuclear magneton, g_{I_a} is the Landé factor for the iodine nucleus, and $C_2=\frac{1}{2}eQ_{I_a}$ is the nuclear electric quadrupole moment with e the proton charge and Q_{I_a} defined as

$$Q_{I_a}=e\langle I_a,M_{I_a}=I_a|\sum_p (3z_p^2-r_p^2)|I_a,M_{I_a}=I_a\rangle, \tag{6}$$

where z_p and r_p refer to the coordinates of the protons p in the iodine nucleus.

For $\Omega\neq 0$, the projection of the angular momentum J onto the molecular axis can take either the positive or the negative direction, a degeneracy that is lifted by the coupling with external states. In this case the molecular wave function is represented by[24]

$$|\psi_\epsilon\rangle=\left(\frac{1}{\sqrt{2}}\right)^{|\epsilon|}[|\Omega,\mathcal{P}JIFM_F\rangle+\epsilon|-\Omega,\mathcal{P}JIFM_F\rangle], \tag{7}$$

where ϵ can take on the values of 0 ($\Omega=0$) and ± 1 ($\Omega>0$). The net effect of this Ω doubling on the matrix element $\langle\psi'_{\epsilon'}|H^k_{\rm hf}(a)|\psi_\epsilon\rangle$ is to replace the $f_k(a,\Omega',v'_{J'},\Omega,v_J)$ defined in Eq. (5) by

$$\left(\frac{1}{\sqrt{2}}\right)^{|\epsilon|+|\epsilon'|}\{[1+\epsilon\epsilon'(-1)^{\Delta J}]f_k(a,\Omega',v'_{J'},\Omega,v_J) + C(\Omega^+)[\epsilon+\epsilon'(-1)^{\Delta J}]f_k(a,\Omega',v'_{J'},-\Omega,v_J)\}, \tag{8}$$

where

$$C(\Omega^+)=\frac{\begin{pmatrix} J' & k & J \\ -\Omega' & \Omega^+ & -\Omega \end{pmatrix}}{\begin{pmatrix} J' & k & J \\ -\Omega' & \Delta\Omega & \Omega \end{pmatrix}}$$

and $\Omega^+=\Omega'+\Omega$. Expression (8) is equivalent to Eq. (6) in Ref. 24 when $\epsilon\neq 0$. For the case of the $B0^+_u$ state, expression (8) is reduced to

$$\left(\frac{1}{\sqrt{2}}\right)^{|\epsilon'|}[1+\epsilon'(-1)^{\Delta J}]f_k(a,\Omega',v'_{J'},0^+_u,v_J). \tag{9}$$

The matrix element for the second nucleus b is related to that of the first nucleus a because of symmetry considerations[24,28]:

$$\langle\psi'_{u,I'}|H^k_{\rm hf}(b)|\psi_{u,I}\rangle=(-1)^{\Delta I}\langle\psi'_{u,I'}|H^k_{\rm hf}(a)|\psi_{u,I}\rangle,$$

$$\langle\psi'_{u,I'}|H^k_{\rm hf}(b)|\psi_{g,I}\rangle=(-1)^{\Delta I+1}\langle\psi'_{u,I'}|H^k_{\rm hf}(a)|\psi_{g,I}\rangle, \tag{10}$$

where the u (g) symmetry refers to the odd (even) electronic wave functions under reflection with respect to the center of the molecule. Another component capable of coupling external electronic states to the $B0^+_u$ state is the off-diagonal part of the rotational Hamiltonian V^0, defined as

$$V^0=-\frac{\hbar^2}{2\mu R^2}[J_+(L_-+S_-)+J_-(L_++S_+)], \tag{11}$$

where μ is the reduced mass of two nuclei and R is the internuclear separation. It can couple only states with $\Delta\Omega=\pm 1$ and the same u (g) symmetry, and therefore the $B0^+_u$ state is coupled by V^0 to only two 1_u states. The matrix element of V^0 between the $B0^+_u$ state and such a 1_u state with Ω doubling ($\epsilon'=1$) is evaluated as

$$\begin{aligned}\langle V^0\rangle&=\langle 1_{u,\epsilon'=1}|V^0|0^+_u\rangle\\ &=-[2J(J+1)]^{1/2}\frac{1}{\sqrt{2}}\\ &\quad\times\left[\left\langle 1_u(\Omega'=1),v'_{J'}\left|\frac{\hbar^2}{2\sqrt{2}\mu R^2}(L_++S_+)\right|0^+_u v_J\right\rangle\right.\\ &\quad\left.+\left\langle 1_u(-\Omega'),v'_{J'}\left|\frac{\hbar^2}{2\sqrt{2}\mu R^2}(L_-+S_-)\right|0^+_u v_J\right\rangle\right]\\ &=-[2J(J+1)]^{1/2}\sqrt{2}\\ &\quad\times\left\langle 1_u(\Omega'=1),v'_{J'}\left|\frac{\hbar^2}{2\sqrt{2}\mu R^2}(L_++S_+)\right|0^+_u v_J\right\rangle\\ &=-[2J(J+1)]^{1/2}\sqrt{2}f_0(1_u,0^+_u).\end{aligned} \tag{12}$$

The factor $\sqrt{2}$ in the last line of Eq. (12) arises from the Ω doubling of the 1_u state.

B. Second-Order Contributions to Hyperfine Parameters

With the coupling matrix elements for V^0, V^1, and V^2 given in Subsection 2.A, the hyperfine parameters are calculated by second-order perturbation theory to include the contributions from all rovibrational levels allowed by the selection rules in each of the six perturbing states [C: 1_u, 1_u, $1_g(^1\Pi_g)$, $1_g(^3\Sigma^-_g)$, $0^-_g(^3\Pi_g)$, and $(3)0^-_u$]. In the derivation of these parameters (see Appendix I in Ref. 28), a weak J' dependence of $f_k(a,\Omega',v'_{J'},\Omega,v_J)$ across neighboring rotational levels is assumed when the summation on J' is performed. However, to account for the Ω doubling, one must replace $f_k(a,\Omega',v'_{J'},\Omega,v_J)$ defined in Eq. (5) with expression (9). In fact, this modification does not interfere with the just-mentioned assumption because the coupling selection rules for $\Delta J=J'-J$ are different for $\epsilon'=+1$ and -1; hence their combined effect adds no extra J' dependence to the modified $f_k(a,\Omega',v'_{J'},\Omega,v_J)$. After summations on I' and J' and reorganization of various terms according to their angular momentum dependence, the explicit expressions for the four effective parameters are obtained and are listed below[28]:

$$C_B = C_D - \frac{4}{[I_a(I_a+1)(2I_a+1)]^{1/2}} \times \sum_{1_u}\left[\sum_{v'}\frac{f_0(1_u,0_u^+)f_1(a,0_u^+,1_u)}{E_{0_u^+vJ}-E_{1_uv'J}} + \frac{2}{\pi}\left(\frac{\mu}{2\hbar^2}\right)^{1/2}\int_{E_0}^{\infty} dE_{1_uJ}\frac{f_0(1_u,0_u^+)f_1(a,0_u^+,1_u)}{\sqrt{E_u}(E_{0_0^+vJ}-E_{1_uJ})}\right], \quad (13)$$

$$\delta_B = -\frac{2}{3I_a(I_a+1)(2I_a+1)} \times \sum_{\Omega'}\chi_i(1+|\epsilon'|)\left[\sum_{v'}\frac{|f_1(a,\Omega',0_u^+)|^2}{E_{0_u^+vJ}-E_{\Omega'v'J}} + \frac{2}{\pi}\left(\frac{\mu}{2\hbar^2}\right)^{1/2}\int_{E_0}^{\infty} dE_{\Omega'J}\frac{|f_1(a,\Omega',0_u^+)|^2}{\sqrt{E_u}(E_{0_u^+vJ}-E_{\Omega'J})}\right], \quad (14)$$

$$d_B = -\frac{1}{3I_a(I_a+1)(2I_a+1)} \times \sum_{\Omega'}\chi_i(3\Omega'^2-2)(1+|\epsilon'|)\left[\sum_{v'}\frac{|f_1(a,\Omega',0_u^+)|^2}{E_{0_u^+vJ}-E_{\Omega'v'J}} + \frac{2}{\pi}\left(\frac{\mu}{2\hbar^2}\right)^{1/2}\int_{E_0}^{\infty} dE_{\Omega'J}\frac{|f_1(a,\Omega',0_u^+)|^2}{\sqrt{E_u}(E_{0_u^+vJ}-E_{\Omega'J})}\right], \quad (15)$$

$$eqQ_B = eqQ_0 - 4\sqrt{2}\sum_{1_u}\left[\sum_{v'}\frac{4f_0(1_u,0_u^+)f_2(a,0_u^+,1_u)}{E_{0_u^+vJ}-E_{1_uv'J}} + \frac{2}{\pi}\left(\frac{\mu}{2\hbar^2}\right)^{1/2}\int_{E_0}^{\infty} dE_{1_uJ}\frac{4f_0(1_u,0_u^+)f_2(a,0_u^+,1_u)}{\sqrt{E_u}(E_{0_u^+vJ}-E_{1_uJ})}\right] + 10\sum_{k',k=1,2}\sum_{\Omega'}(-1)^{2I_a+\Omega'}(1+|\epsilon'|) \times \left[\sum_{v'}\frac{2f_k^*(a,\Omega',0_u^+)f_{k'}(a,\Omega',0_u^+)}{E_{0_u^+vJ}-E_{\Omega'v'J}} + \frac{2}{\pi}\left(\frac{\mu}{2\hbar^2}\right)^{1/2} \times \int_{E_0}^{\infty} dE_{\Omega'J}\frac{2f_k^*(a,\Omega',0_u^+)f_{k'}(a,\Omega',0_u^+)}{\sqrt{E_u}(E_{0_u^+vJ}-E_{\Omega'J})}\right] \times \begin{pmatrix} k & k' & 2 \\ \Delta\Omega & -\Delta\Omega & 0\end{pmatrix}\begin{Bmatrix} I_a & 2 & I_a \\ k & I_a & k'\end{Bmatrix}\begin{Bmatrix} 2 & I_a & I_a \\ 0 & I_a & -I_a\end{Bmatrix}. \quad (16)$$

C_D and eqQ_0 are the first-order contributions to the corresponding parameters in Eqs. (13) and (16), respectively. In Eqs. (14)–(16), $\Omega' \geq 0$ and ϵ' can take on the values of $0(\Omega'=0)$ and $\pm 1(\Omega'>0)$. For each perturbing electronic state Ω', $\chi_i = 1$ (-1) if the state has g (u) symmetry and the state's contribution to the hyperfine parameters comes from both discrete levels (v', J) and the energy continuum E_J, whose density of state is $(2/\pi)(\mu/2\hbar^2 E_u)^{1/2}$, where E_u is the radial kinetic energy. E_0, the lower limit of the integrals for the energy continuum, is the energy just above the last discrete rovibrational level that an attractive potential can support. In the expressions for δ_B, d_B, and eqQ_B, the extra factor $(1+|\epsilon'|)$ arises from the Ω doubling of the perturbing state Ω'.

C. Preparation of Potential Energy Curves and Electronic Wave Functions

We use the available empirical and theoretical I_2 PECs to construct the rovibrational structure and the associated wave functions inside each electronic state. The B-state empirical PEC is adopted from the analysis performed by Gerstenkorn *et al.*,[29] in which the PEC was constructed from Fourier spectroscopic data by use of an inverted perturbation approach method. For the six states that perturb the $B0_u^+$ state, we adopt the empirically improved relativistic PECs in Ref. 30, and these PECs are used in the short and intermediate internuclear separations ($R \leq 6.5$ Å). Figure 1 plots these PECs over the range 2.5 Å $< R < 6.5$ Å, along with the B-state empirical PEC and the other three PECs belonging to the same dissociation limit. Apart from these PECs, the $1_g(^1\Pi_g)$ empirical PEC determined from the optical–optical double-resonance experiment by Jewsbury *et al.*[31] is also tested in the calculation. For large internuclear separations ($R > 7$ Å), the PECs take the inverse-power form, $V(R) = (C_5/R^5) + (C_6/R^6) + E_{\rm diss}$, which includes quadrupolar electrostatic and dispersion energy terms, with the corresponding coefficients C_5 and C_6 determined by Saute and Aubert-Frécon.[32] Figure 2 shows these long-range PECs for all ten electronic states that share the same dissociation limit, $^2P_{3/2} + {}^2P_{1/2}$. To make a smooth transition between the two PEC segments, each short-range PEC is shifted vertically to match the corresponding long-range PEC at around $R = 7$ Å. The matched short- and long-range PECs are illustrated in Fig. 3.

The matrix element $\langle \Omega' v_J' | V_{\Delta\Omega}^k(a) | 0_u^+ v_J \rangle$ in the functions $f_k(a, \Omega', 0_u^+)$ in Eqs. (13)–(16) is approximated as a product of an electronic matrix element and a Franck–Condon in-

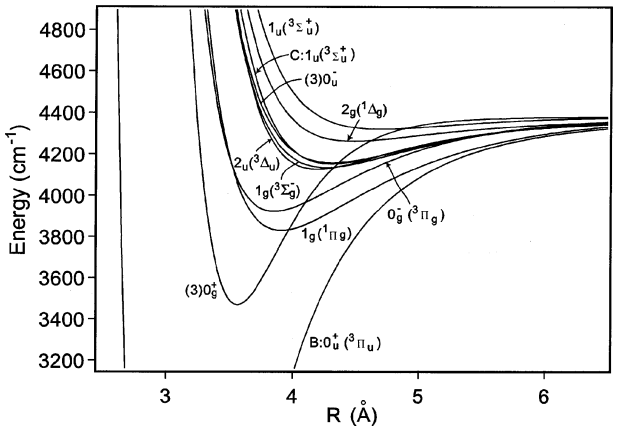

Fig. 1. PECs for ten electronic states converging to the $^2P_{3/2} + {}^2P_{1/2}$ dissociation limit over the range 2.5 Å $< R < 6.5$ Å. These PECs are adopted from the relativistic calculations by de Jong *et al.*[30] except for the B state, for which an empirical PEC[29] is used.

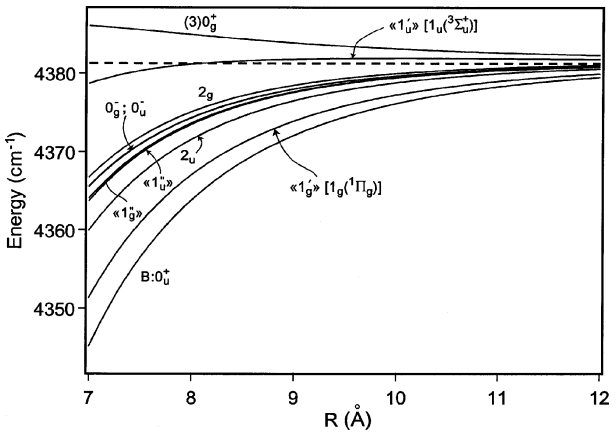

Fig. 2. Long-range PECs for the ten electronic states, adopted from Ref. 32. Dashed line, the $^2P_{3/2}+^2P_{1/2}$ dissociation limit. Note that $1_u''$ and $1_g''$ refer to the $C{:}1_u(^3\Sigma_u^+)$ and $1_g(^3\Sigma_g^-)$ states, respectively.

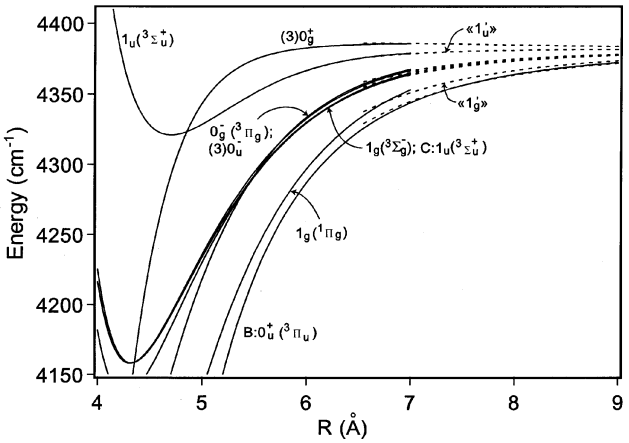

Fig. 3. Combining the short- and long-range potentials. Solid curves, the short-range ($R<7$ Å) PECs from the *ab initio* calculation[30]; dashed curves, the *ab initio* long-range PECs from Ref. 32. To make a smooth connection between two segments of the PEC, each short-range ($R<7$ Å) PEC has been shifted vertically to match the corresponding long-range one. The unchanged B-state empirical PEC[29] and *ab initio* long-range PEC are also included.

tegral between the $B0_u^+$ and the perturbing states. The electronic matrix element is assumed to have a weak R dependence over the range sampled by the vibrational wave function. FORTRAN codes LEVEL[33] and BCONT[34] developed by Le Roy and Kraemer are used to calculate the Franck–Condon integrals for the discrete levels and energy continua, respectively. As an example, a portion of the B-state rovibrational structure is sketched in Fig. 4, and the vibrational levels inside a perturbing state $C{:}1_u$ are shown in Fig. 5. A special case arises when a potential can support rotational levels above its asymptotic energy because of a potential barrier located at the PEC outer limb. Wave functions of such levels can tunnel through the potential barrier. As a result, their energy spectra can be broadened significantly and can no longer be treated as discrete or quasi-discrete levels. We isolate these levels from the rest of the discrete levels and treat them instead as part of the energy continuum.

At large internuclear separations ($R>\sim 7$ Å), the molecular wave functions can be constructed from symmetrized products of two atomic wave functions. Each molecular wave function constructed in this way is a linear combination of the separated-atom basis functions (see Table I in Ref. 32). For example, the two 1_u states, $1_u(^3\Sigma_u^+)$ and $C{:}1_u(^3\Sigma_u^+)$, also designated as $1_u'$ and $1_u''$, respectively, are mixtures of the two basis functions $|1_u'\rangle$ and $|1_u''\rangle$:

$$|1_u'\rangle = \alpha|1_u'\rangle - \sqrt{1-\alpha^2}|1_u''\rangle,$$

$$|1_u''\rangle = \alpha|1_u''\rangle + \sqrt{1-\alpha^2}|1_u'\rangle, \tag{17}$$

with α as the admixture of the two basis functions. Likewise, the two 1_g states, $1_g(^1\Pi_g)$ and $1_g(^3\Sigma_g^-)$, are linear combinations of the two basis functions $|1_g'\rangle$ and $|1_g''\rangle$:

$$|1_g'\rangle = \beta|1_g'\rangle + \sqrt{1-\beta^2}|1_g''\rangle,$$

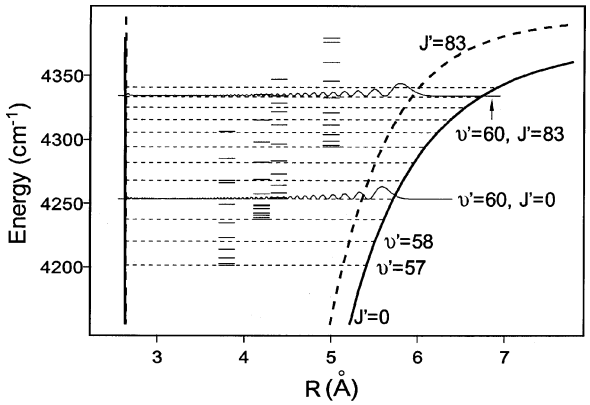

Fig. 4. B-state rovibrational structure. Thick solid curves are the empirical B-state rotationless potential.[29] Vibrational levels $v'=57-68$ are indicated as short-dashed lines. The rotational levels at several vibrational levels are also drawn as short bars. The curve of long dashes is the effective potential (a sum of the rotationless and centrifugal potentials) associated with a rotational level ($v'=60, J'=83$). The probability distributions of the molecular vibration for levels ($v'=60, J'=0$) and ($v'=60, J'=83$) are plotted as thin solid curves for comparison of the internuclear separations populated by the two levels.

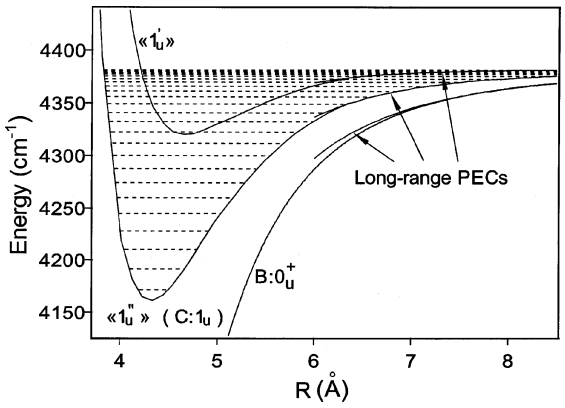

Fig. 5. Two 1_u PECs used in the calculation of C_B. Also plotted is the B-state empirical potential,[29] which is used for all internuclear separations. $C{:}1_u$ and 1_u PECs ($R<7$ Å) are constructed from theoretical[30] ($R<7$ Å) and long-range PECs[32] ($R\geqslant 7$ Å). The PECs from *ab initio* calculation are shifted vertically to match the corresponding long-range ones. Dashed lines, the vibrational levels of the $C{:}1_u$ state. The 1_u and $C{:}1_u$ states are also denoted by $1_u'$ and $1_u''$, respectively.

$$|1_g''\rangle = \beta|1_g''\rangle - \sqrt{1-\beta^2}|1_g'\rangle, \tag{18}$$

where $1_g'$ and $1_g''$ refer to $1_g(^1\Pi_g)$ and $1_g(^3\Sigma_g^-)$ states, respectively. The R dependence of the mixing parameters α and β will be examined in Section 3. The other two states, $0_g^-(^3\Pi_g)$ and $(3)0_u^-$, each consist of only one basis function. With molecular wave functions derived from the separated-atomic basis functions, the electronic matrix element $\langle\Omega'|V^k_{\Delta\Omega}(a)|0_u^+\rangle$ can be readily determined from the experimental values of atomic hyperfine constants.[18,24]

3. RESULTS AND DISCUSSIONS

In this section we present results for the calculated effective hyperfine parameters, eqQ_B, C_B, d_B, and δ_B, together with a detailed analysis of the electronic structure of the associated states. The calculation covers nearly all the vibrational levels ($3 \leqslant v' \leqslant 82$) in the $B0_u^+$ state, with R_c extending from $\sim$3.5 to $\sim$12.5 Å. Additionally, to demonstrate the numerical analysis on a finer energy scale, we show the calculated rotational dependence of the hyperfine parameter C_B for two vibrational levels. We also compare calculations with experimental results.

A. Spin–Rotation Parameter C_B and the Admixture of Two 1_u States

The states that contribute to C_B are restricted to the 1_u states by the coupling selection rule associated with the off-diagonal rotational Hamiltonian V^0. Thus the calculation of C_B automatically isolates the second-order contributions of the two 1_u states from those of the other four perturbing states. Furthermore, this allows a determination of the mixing parameter α between the two 1_u states that, in turn, can serve as a consistency check of the relevant *ab initio* calculation based on the separated-atom model. The details of the PECs and molecular wave functions used in Eq. (13) have already been described in Section 2. Here we stress that, in the calculation, we are able to use the same value for mixing parameter α at a wide range of internuclear separations, especially in the intermediate and long ranges and this value is adjusted until a global agreement with experimental data is achieved.

Figure 6 summarizes the comparison between calculations and experiments. In the figure, filled circles are experimental data, and open circles and squares are calculations performed with the mixing parameter $\alpha = 0.99$ and 0.9, respectively. To the best of our knowledge, we incorporated all available experimental data reported in previous publications.[1–17] First, the result shows a sensitive dependence on the mixing parameter α at large internuclear separations $R > \sim 7$ Å, as shown in Fig. 6(a). In contrast, we verify that the uncertainty in the two 1_u PECs has merely a small influence on the calculation at large R. For instance, we intentionally decrease the potential depths of the two 1_u states by 50 and 30 cm^{-1} and repeat the calculation. While this modification results in a noticeable reduction of C_B between 4.0 and 5.5 Å, as indicated by triangles in Fig. 6(b), it induces less than a 2% change of C_B at $R_c > \sim 7$ Å. Additional diagnostic tests on the different parts of the two 1_u PECs produce similar outcomes. Consequently, the mixing parameter α is essentially constant and takes on the value of 0.99 for internuclear separation $R > 7$ Å. Moreover, a calculation that uses the same α at even shorter R_c is in good agreement with the experiment until R_c reaches 4 Å, as shown in Figs. 6(b) and 6(c). On the other hand, a close examination of C_B at $R_c < 4$ Å in Fig. 6(c) shows that the calculated results gradually deviate from the experiment, quantitatively illustrating a transition from the separated-atom model to the overlapped and distorted charge distribution that calls for a description employing more sophisticated molecular wave functions.

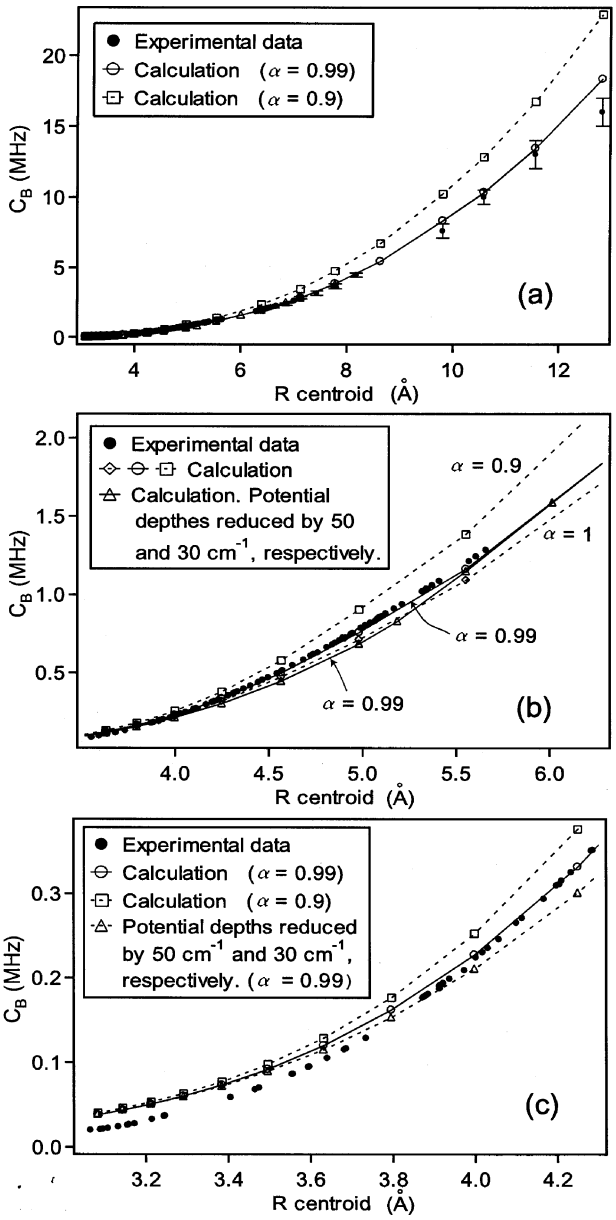

Fig. 6. Second-order calculations of the spin–rotation parameter C_B. Filled circles, spectroscopic data from the literature[1–17]; other symbols and lines, calculations. (a) With a mixing parameter $\alpha = 0.99$ (open circles on solid curve) for two 1_u states, the calculations agree well with the experimental data,[1–17] whereas changing α to 0.9 (squares on dashed curve) results in a large global deviation from the experimental data. (b) A deliberate reduction of the potential depths of the two 1_u PECs (triangles on solid curve) produces a noticeable discrepancy at $R_c = 4.2$–5.5 Å but does not affect calculations at shorter and longer internuclear separations. (c) At $R_c < \sim 4$ Å, the calculation begins to depart from the experimental data.[1–17]

Figure 7 plots the calculated rotational dependence for two vibrational levels, $v'=70$ and $v'=47$, with the mixing parameter $\alpha=0.99$. Considering a large energy difference between the two levels and the use of a fixed mixing parameter, the agreement with the experimental data[1–17] is reasonably good at both vibrational levels. Similar to the global trend exhibited in Fig. 6, the rotational dependence of C_B is due to the smooth variation of the Franck–Condon overlap and the energy denominator in Eq. (13). This variation is also responsible for the perturbation-induced rovibrational dependence in the other three hyperfine parameters.

When dealing with high-lying levels of the $B0_u^+$ state, we estimate the possible contributions beyond second-order perturbation theory. The strength of the perturbation is characterized by the parameter $\lambda=|\eta/\Delta E|$, where η is the coupling between the two discrete levels inside the $B0_u^+$ and 1_u states and ΔE is their energy difference. Numerical estimation shows that λ is well below 1 for these high-lying levels. Moreover, when there is a possibility of energy coincidence, magnitude of the coupling between the two levels involved is verified to be below a few megahertz. Given this coupling strength, ΔE has to be less than a few tens of megahertz for a strong perturbation to occur, which is unlikely because of the large mismatch in the rovibrational constants of the $B0_u^+$ and 1_u states. Thus second-order perturbation theory is sufficient for the calculation of C_B and the analysis of the related 1_u states. However, for the other three hyperfine parameters, precautions should be taken because the $B0_u^+$ state can be strongly coupled to a discrete level in a particular electronic state. We will discuss this case in Subsection 3.C.

B. Separation of Contributions from $0_g^-(^3\Pi_g)$ and $(3)0_u^-$ States

Although only two 1_u states contribute to C_B, the other three parameters, δ_B, d_B, and eqQ_B, contain perturbations from all six perturbing states. In Subsection 3.A, we determined the mixing parameter α associated with the two 1_u states, and the sensitivity of C_B to the related PECs was investigated. With the help of this information, we decompose the hyperfine parameters into contributions from subsets of six states, or even from individual states when it is possible, allowing a sensitive characterization of the 0_g^- and 0_u^- states and the related long-range potentials.

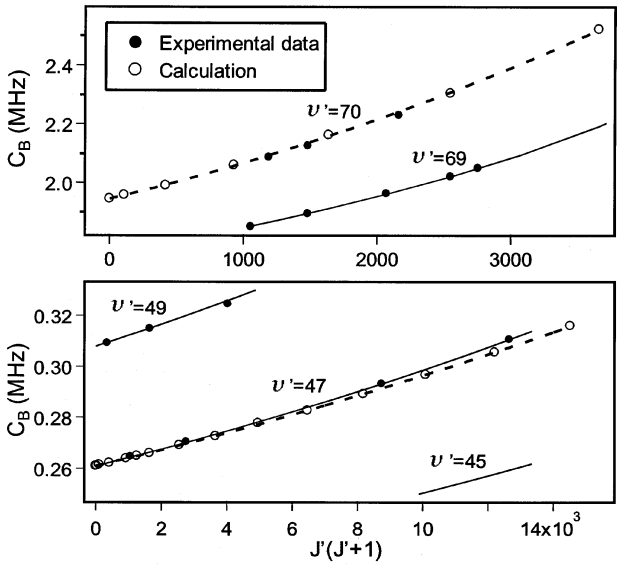

Fig. 7. Rotational dependence of C_B around two vibrational levels $v'=47$ and 70. Filled circles and solid curves, experimental data[1–17] and fit, respectively. Open circles, calculation by second-order perturbation theory. Dashed curves, fits to the computed points.

We divide the six states into four groups: two 1_u states, the 0_g^- state, the 0_u^- state, and two 1_g states. Each of the three hyperfine parameters can be decomposed into terms that correspond to the contributions from these four groups of electronic states. For instance, the scalar spin–spin parameter δ_B can be written as

$$\delta_B=\delta(1_u)+\delta(1_g)+\delta(0_g^-)+\delta(0_u^-). \tag{19}$$

From Eqs. (14) and (15), it follows that d_B is closely related to δ_B by

$$d_B=\tfrac{1}{2}\delta(1_u)+\tfrac{1}{2}\delta(1_g)-\delta(0_g^-)-\delta(0_u^-). \tag{20}$$

Using Eqs. (19) and (20), we can isolate the contributions of the 0_g^- and 0_u^- states from those of the other four states by

$$[\delta(0_g^-)+\delta(0_u^-)]=\tfrac{1}{3}(\delta_B-2d_B), \tag{21}$$

where the right-hand side can be determined experimentally with the values of δ_B and d_B extracted from the spectroscopic fit.[1–17] The left-hand side of Eq. (21) is calculated and plotted (open squares on dashed curve) in Fig. 8(a). For comparison we also plot the experimental values (filled circles) according to the right-hand side of Eq. (21). Recall that in the calculation there is no adjustable parameter for the electronic wave functions of the 0_g^- and 0_u^- states. As can be seen in Fig. 8(a), there is a noticeable discrepancy between the experiment and the calculation, which increases with increasing R_c.

To resolve the source of this discrepancy, the contributions from 0_g^- and 0_u^- need to be distinguished from each other. We notice that the last term in Eq. (16) for eqQ_B dominates when k and k' equal 1. Thus one can keep only these terms and compare them with Eq. (14). This leads to the following relation between eqQ_B and δ_B:

$$\tfrac{1}{20}[eqQ_B-eqQ_0]\approx-\tfrac{1}{2}\delta(1_u)+\tfrac{1}{2}\delta(1_g)-\delta(0_g^-)+\delta(0_u^-), \tag{22}$$

where eqQ_0 is the first-order contribution, which is calculated in the separated-atom basis set at large internuclear separations. From Eqs. (19) and (20) and expression (22), the contributions from 0_g^- and 0_u^- are thus isolated from each other by

$$[\delta(1_u)-2\delta(0_u^-)]=d_B-\tfrac{1}{20}(eqQ_B-eqQ_0),$$

$$[\delta(1_u)+2\delta(0_g^-)]=\tfrac{2}{3}\delta_B-\tfrac{1}{3}d_B-\tfrac{1}{20}(eqQ_B-eqQ_0), \tag{23}$$

where the right-hand side again can be determined experimentally by use of the values of δ_B, d_B, and eqQ_B extracted from the spectroscopic fit. In Subsection 3.A we

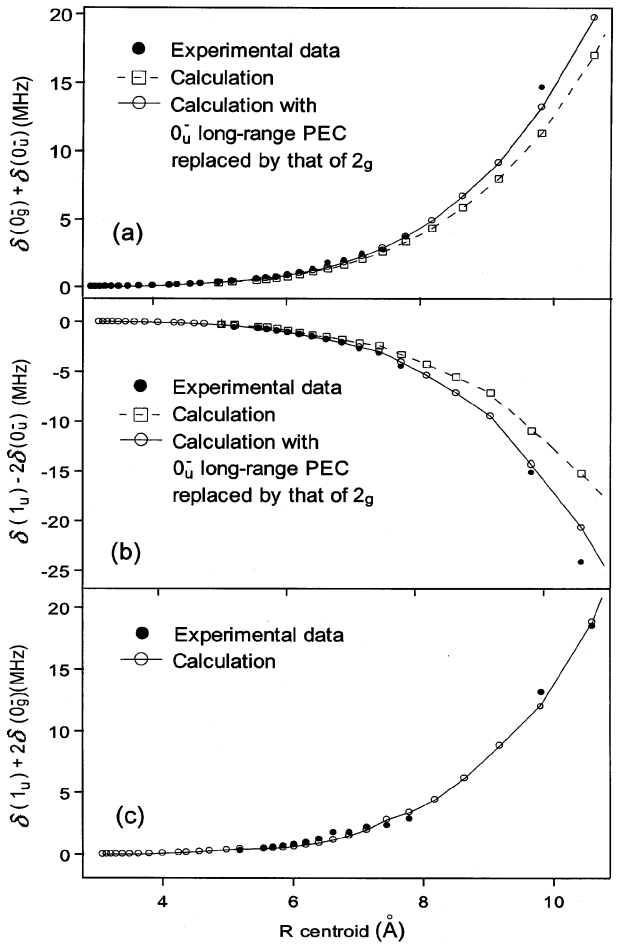

Fig. 8. Separation of the contributions from the 0_u^- and 0_g^- states. (a), The overall contribution of the 0_u^- and 0_g^- states to δ_B. (b) and (c), Two separated contributions. Filled circles, values deduced from the experimental data[1–17] on δ_B, d_B, and eqQ_B [see Eqs. (21) and (23) and text for details]. Open squares on dashed curves, the calculations; open circles on solid curves, the calculation with the 0_u^--long-range PEC replaced by that of the 2_g state (see Fig. 2 for the two long-range PECs). In this calculation, there is no adjustable parameter for the electronic wave functions.

determined the mixing parameter α related to 1_u states. This information is incorporated into the calculation of the left-hand side of Eqs. (23) that also involves the contribution from two 1_u states. Figures 8(b) and 8(c) show our results for the 0_g^- (open squares on dashed curves) and 0_u^- (open circles) states, respectively, along with the experimental data (filled circles) plotted in both panels according to the right-hand side of Eqs. (23). While the calculation of 0_g^- agrees with experimental data, a discrepancy exists for the 0_u^- state that is consistent with the discrepancy observed in Fig. 8(a). Evidently, the calculation of 0_u^- is the source of this discrepancy.

We perform additional diagnostic calculations of $\delta(0_u^-)$. We verify that moderate modifications to the short- and intermediate-range potentials of the 0_u^- state cannot be responsible for the large discrepancy at $R_c > \sim 8$ Å, as shown in Fig. 8(b). Conversely, $\delta(0_u^-)$ is sensitive to C_5 and C_6 of the 0_u^- long-range potential. In fact, at large R_c, the magnitude of $\delta(0_u^-)$ has a steep increase that is dominated by perturbations from the last few discrete levels in the 0_u^- state whose energies depend sensitively on the shape of the long-range potential. We therefore adjust C_5 and C_6 of the 0_u^- long-range potential to compensate for the error in the calculation of $\delta(0_u^-)$. The modified long-range potential is then close to the 2_g long-range potential as shown in Fig. 2. In light of this observation, we repeat the calculation of $\delta(0_u^-)$ with the 0_u^- long-range potential replaced with that of the 2_g state. These new results (open circles on the solid curve) are also presented in Figs. 8(a) and 8(b). The discrepancy is greatly reduced in comparison with the dashed curves that used the original 0_u^- long-range potential. We also estimate the coupling-strength λ introduced in Subsection 3.A for each discrete level in the 0_u^- state to confirm the validity of the above analysis by use of second-order perturbation theory. We note that, although this comparison demonstrates a highly sensitive dependence of hyperfine interactions on the long-range PEC, the analysis alone does not provide a definitive answer to the preferred use of the 2_g-state long-range PEC.

C. Strong Perturbation from the $1_g(^1\Pi_g)$ State and Its Contributions to Hyperfine Parameters δ_B, d_B, and eqQ_B

In previous subsections we divided the six perturbing states that contribute to δ_B, d_B, and eqQ_B into four groups, and the contributions from three groups were analyzed in detail. Once the contributions from the last two 1_g states are determined, the three hyperfine parameters δ_B, d_B, and eqQ_B can be obtained by combination of contributions from all four groups. Among the two 1_g states, the outer branch of the $1_g(^1\Pi_g)$ PEC is close to that of the $B0_u^+$ state (see Figs. 1 and 2), resulting in a strong coupling to high-lying levels ($70 \leqslant v_B' \leqslant 82$) of the $B0_u^+$ state because of favorable Franck–Condon overlaps.[4] Furthermore, this perturbation is enhanced because for each high-lying level in the $B0_u^+$ state, there is a nearby discrete level in the $1_g(^1\Pi_g)$ state whose energy separation with the perturbed level is typically a few gigahertz. In calculating the contribution of the 1_g states, we monitor the coupling strength between the $B0_u^+$ and $1_g(^1\Pi_g)$ states for high-lying levels ($70 \leqslant v_B' \leqslant 82$). For $v_B' \leqslant 78$, the coupling-strength λ is verified to be below 0.1, whereas at the last four levels $v_B' = 79-82$, λ can be as large as 0.4. Therefore the second-order calculation for the $1_g(^1\Pi_g)$ state is primarily restricted to levels below $v_B' = 78$.

Despite the inadequacy of the second-order calculation for the $1_g(^1\Pi_g)$ perturbation allows a high-resolution examination of the $1_g(^1\Pi_g)$ long-range potential. We find that only a minor adjustment on the long-range PEC (see Fig. 2) is needed for the calculation of δ_B to achieve good agreement with the experimental data,[1–17] as shown in Fig. 9. In the calculation the value of the mixing parameter β for the two 1_g states is taken from Ref. 4 and kept fixed.

Considering the linear independence of Eqs. (19) and (20) and expression (22), we perform calculations of d_B and eqQ_B to cross-check the 1_g long-range PEC and the mixing parameters α and β. The hyperfine parameter d_B is calculated with Eq. (20). In the case of eqQ_B, our calculation includes both major contributions in expression (22) and other minor terms in Eq. (16). The results for d_B and eqQ_B agree reasonably well with experiment, as

shown, respectively, in Figs. 10 and 11. Compared with d_B, our calculation of eqQ_B has a relatively large discrepancy because the residual error of $\delta(1_g)$ is amplified by a factor of 10 in the case of eqQ_B according to Eq. (19) and expression (22). Once the mixing parameter β of the two 1_g states is independently determined, the calculation of d_B and eqQ_B can be further improved by a global fit of the $1_g(^1\Pi_g)$ long-range PEC to the three hyperfine parameters δ_B, d_B, and eqQ_B.

Unlike C_B, δ_B, and d_B, which result solely from perturbations of external electronic states over the whole range of internuclear separation, eqQ_B has both first-order and second-order components that are important in different regions. Our numerical analysis makes it possible to locate more accurately the regions at which each component dominates. As shown in Fig. 11, at short internuclear separation ($R_c < 5$ Å), the perturbation from the external states is negligible. The perturbation sets in at $R_c \sim 5$ Å and increases along with the internuclear separation. Finally, it is worth noting that, at $R_c < 5$ Å, the first-order component of eqQ_B departs from the constant value determined by both the separated-atom basis and the linear combination of atomic orbitals models with the decreasing internuclear separation because of a combined effect of (1) the nuclear quadrupole–quadrupole interaction and (2) the distortion and overlapping of the two atomic electric charge distributions.

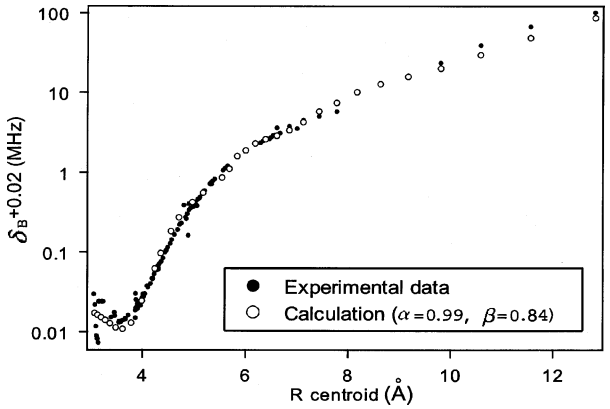

Fig. 9. Semilogarithmic plot of the second-order calculation of the scalar spin–spin parameter δ_B. Filled circles, experimental data[1–17]; open circles, calculations. In the calculation, the mixing parameters for the two 1_u and the two 1_g states are fixed to $\alpha = 0.92$ and $\beta = 0.84$, respectively. Because the contribution from $1_g(^1\Pi_g)$ state is extremely sensitive to the corresponding long-range potential, the $1_g(^1\Pi_g)$ long-range potential is fine tuned (see Fig. 2) to obtain good agreement with the experimental data.[1–17]

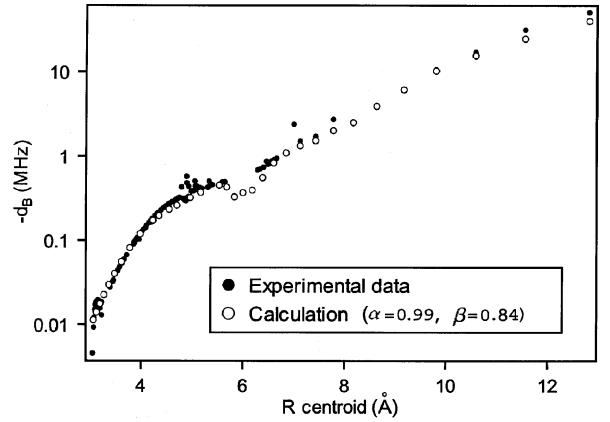

Fig. 10. Semilogarithmic plot of the second-order calculation of the tensor spin–spin parameter d_B. Filled circles, experimental data[1–17]; open circles, calculations. The calculation combines the contributions from all six states [see Eq. (20)] that are determined in the calculation of δ_B. The calculation provides a cross-check of the 1_g long-range PEC and the mixing parameters α and β.

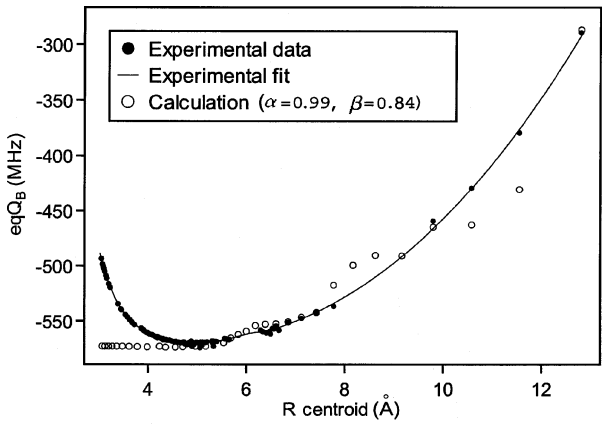

Fig. 11. Second-order calculation of the electric quadrupole parameter eqQ_B. Filled circles, experimental data[1–17]; open circles, calculations. The calculation combines the contributions from the same six states used for Figs. 9 and 10. The calculation provides a cross-check of the 1_g long-range PEC and the mixing parameters α and β. The relatively large discrepancy is due to the fact that the residual error of $\delta(1_g)$ (the contribution of the 1_g states to δ_B) has been amplified by a factor of 10 in the case of eqQ_B [see Eq. (19) and expression (22)].

4. CONCLUSIONS

We have performed second-order calculations of the four hyperfine parameters C_B, δ_B, d_B, and eqQ_B by using the available molecular PECs and electronic wave functions derived from the separated-atom basis set. We have shown that, by dividing the six perturbing electronic states into four subgroups, their contributions to the hyperfine parameters can be separated and directly compared with the corresponding experimental data. For the spin–rotation parameter C_B, the results for both rovibrational dependence agree well with the experimental data for a wide range of internuclear separations ($R_c > \sim 4$ Å), and the admixture of the two 1_u states is independently determined as $\alpha = 0.99$. However, the calculations depart from the experimental data at short internuclear separations ($R_c < \sim 4$ Å), indicating the breakdown of the separated-atom model. Moreover, calculations of the other three hyperfine parameters verify the mixing parameter of two 1_g states and place a stringent constraint on the long-range PECs of the relevant electronic states. On the basis of our investigations described here and earlier studies,[1–17] the effective hyperfine Hamiltonian developed in Ref. 28 with second-order perturbation is proved to be sufficiently accurate to describe the experimental obser-

vations when strong perturbation from the 1_g state is absent. The study provides an independent and quantitative test on the separated-atom model and the related PECs.

ACKNOWLEDGMENTS

We thank J. L. Hall for his critical reading of the manuscript and W.-Y. Cheng for his contributions at an earlier stage of this paper. We acknowledge support from NASA, the National Science Foundation, the U.S. Office of Naval Research, and the National Institute of Standards and Technology.

L. Chen's e-mail address is lchen@jilau1.colorado.edu, and J. Ye's e-mail address is Ye@jila.colorado.edu

*Permanent address, Pacific Northwest National Laboratory, Richland, Washington 99352.

REFERENCES

1. C. J. Bordé, G. Camy, B. Decomps, and J.-P. Descoubes, "High precision saturation spectroscopy of $^{127}I_2$ with argon lasers at 5145 Å and 5017 Å—main resonances," J. Phys. (France) **42**, 1393–1411 (1981).
2. B. Bodermann, H. Knöckel, and E. Tiemann, "Widely usable interpolation formulae for hyperfine splittings in the $^{127}I_2$ spectrum," Eur. Phys. J. D **19**, 31–44 (2002).
3. H. Knöckel, B. Bodermann, and E. Tiemann, "High precision description of the rovibronic structure of the I_2 $B–X$ spectrum," Eur. Phys. J. D **28**, 199–209 (2004).
4. J. P. Pique, F. Hartmann, S. Churassy, and R. Bacis, "Hyperfine interactions in homonuclear diatomic molecules and $u–g$ perturbations. II. Experiments on I_2," J. Phys. (France) **47**, 1917–1929 (1986).
5. F.-L. Hong, J. Ye, L.-S. Ma, S. Picard, C. J. Bordé, and J. L. Hall, "Rotation dependence of electric quadrupole hyperfine interaction in the ground state of molecular iodine by high-resolution laser spectroscopy," J. Opt. Soc. Am. B **18**, 379–387 (2001).
6. T. J. Quinn, "Practical realization of the definition of the metre (1997)," Metrologia **36**, 211–244 (1999).
7. F. L. Hong and J. Ishikawa, "Hyperfine structures of the $R(122)$ 35–0 and $P(84)$ 33–0 transitions of $^{127}I_2$ near 532 nm," Opt. Commun. **183**, 101–108 (2000).
8. C. S. Edwards, G. P. Barwood, P. Gill, F. Rodriguez Llorente, and W. R. C. Rowley, "Frequency-stabilised diode lasers in the visible region using Doppler-free iodine spectra," Opt. Commun. **132**, 94–100 (1996).
9. C. S. Edwards, G. P. Barwood, P. Gill, and W. R. C. Rowley, "A 633 nm iodine-stabilized diode-laser frequency standard," Metrologia **36**, 41–45 (1999).
10. A. Razet, J. Gagniere, and P. Juncar, "Hyperfine structure analysis of the $33P$ (6–3) line of $^{127}I_2$ at 633 nm using a continuous-wave tunable dye laser," Metrologia **30**, 61–65 (1993).
11. H. R. Simonsen, "Iodine-stabilized extended cavity diode laser at lambda=633 nm," IEEE Trans. Instrum. Meas. **46**, 141–144 (1997).
12. A. Morinaga, K. Sugiyama, and N. Ito, "Hyperfine structure of low-lying vibrational levels in the B-electronic state of molecular iodine," J. Opt. Soc. Am. B **6**, 1656–1659 (1989).
13. P. Gill and J. A. Clancy, "A microprocessor-controlled iodine-stabilized ion laser," J. Phys. E **21**, 213–218 (1988).
14. F. Bertinetto, P. Cordiale, S. Fontana, and G. B. Picotto, "Helium–neon lasers stabilized to iodine at 605-nm," IEEE Trans. Instrum. Meas. **36**, 609–612 (1987).
15. W.-Y. Cheng, J. T. Shy, and T. Lin, "A compact iodine-stabilized HeNe laser and crossover resonances at 543 nm," Opt. Commun. **156**, 170–177 (1998).
16. L. Chen, W.-Y. Cheng, and J. Ye, "Hyperfine interactions and perturbation effects in the $B0_u^+(^3\Pi_u)$ state of $^{127}I_2$," J. Opt. Soc. Am. B **21**, 820–832 (2004).
17. L. Chen and J. Ye, "Extensive, high-resolution measurement of hyperfine interactions: precise investigations of molecular potentials and wave functions," Chem. Phys. Lett. **381**, 777–783 (2003).
18. J. Vigué, M. Broyer, and J. C. Lehmann, "*Ab initio* calculation of hyperfine and magnetic parameters in the I_2 B state," Phys. Rev. Lett. **42**, 883–887 (1979).
19. R. Bacis, M. Broyer, S. Churassy, J. Vergès, and J. Vigué, "eQq measurements in the X, 1_g, 0_g^+ and B state of I_2: a test of the electronic molecular eigenfunctions," J. Chem. Phys. **73**, 2641–2650 (1980).
20. J. P. Pique, R. Bacis, M. Broyer, S. Churassy, and J. B. Koffend, "Calculation of the magnetic hyperfine interaction in the E and X states of iodine with the separated-atom theory," J. Chem. Phys. **80**, 1390–1393 (1984).
21. F. Martin, S. Churassy, R. Bacis, R. W. Field, and J. Vergès, "Long range behavior of the gerade states near the $^2P_{3/2}+{}^2P_{3/2}$ iodine dissociation limit by laser-induced-fluorescence Fourier-transform spectroscopy," J. Chem. Phys. **79**, 3725–3737 (1983).
22. J. P. Pique, F. Hartmann, R. Bacis, and S. Churassy, "Hyperfine structure of higher rovibrational levels in the iodine B state studied by Ar^+ laser induced fluorescence," Opt. Commun. **36**, 354–358 (1981).
23. J. P. Pique, F. Hartmann, R. Bacis, S. Churassy, and J. B. Koffend, "Hyperfine-induced ungerade–gerade symmetry breaking in a homonuclear diatomic molecule near a dissociation limit: $^{127}I_2$ at the $^2P_{3/2}–{}^2P_{1/2}$ limit," Phys. Rev. Lett. **52**, 267–270 (1984).
24. J. P. Pique, F. Hartmann, S. Churassy, and R. Bacis, "Hyperfine interactions in homonuclear diatomic molecules and $u–g$ perturbations. I. Theory," J. Phys. (France) **47**, 1909–1916 (1986).
25. A. Morinaga, "Hyperfine structure and hyperfine coupling constant of molecular iodine," Jpn. J. Appl. Phys., Part 1 **23**, 774–775 (1984).
26. W. S. Barney, C. M. Western, and K. C. Janda, "Measurement of the electronic wave function: separated atom wave function analysis of the R-dependent hyperfine constants of the iodine monochloride A state," J. Chem. Phys. **113**, 7211–7223 (2000).
27. N. F. Ramsey and E. M. Purcell, "Interactions between nuclear spins in molecules," Phys. Rev. **85**, 143L–144L (1952).
28. M. Broyer, J. Vigué, and J. C. Lehmann, "Effective hyperfine hamiltonian in homonuclear diatomic molecules. Application to the B state of molecular iodine," J. Phys. (France) **39**, 591–609 (1978).
29. S. Gerstenkorn, P. Luc, and C. Amiot, "Analysis of the long range potential of iodine in the $B^3\Pi_{0u}^+$ state," J. Phys. (France) **46**, 355–364 (1985).
30. W. A. de Jong, L. Visscher, and W. C. Nieuwpoort, "Relativistic and correlated calculations on the ground, excited, and ionized states of iodine," J. Chem. Phys. **107**, 9046–9058 (1997).
31. P. J. Jewsbury, T. Ridley, K. P. Lawley, and R. J. Donovan, "Parity mixing in the valence states of I_2 probed by optical–optical double-resonance excitation of ion-pair states—characterization of a new ion-pair state, $H1_u(^3P_1)$, and a valence state, $c1_g$," J. Mol. Spectrosc. **157**, 33–49 (1993).
32. M. Saute and M. Aubert-Frécon, "Calculated long-range potential-energy curves for the 23 molecular states of I_2," J. Chem. Phys. **77**, 5639–5646 (1982).
33. R. J. Le Roy, "LEVEL 7.5: a computer program for solving the radial Schrödinger equation for bound and quasibound levels," University of Waterloo Chemical Physics Research Rep. CP-655 (University of Waterloo, Waterloo, Ontario, Canada, 2002). The source code and manual for this program may be obtained from the Computer Programs link on the Internet site http://leroy.uwaterloo.ca.

34. R. J. Le Roy and G. T. Kraemer, "BCONT 2.0. Computer program for calculating absorption coefficients, emission intensities or (golden rule) predissociation rates," University of Waterloo Chemical Physics Research Rep. CP-650 (University of Waterloo, Waterloo, Ontario, Canada, 2001). The source code and manual for this program may be obtained from the internet site http://leroy.uwaterloo.ca.